NIR laser-activated polydopamine-coated Fe_3O_4 nanoparticles used as a novel precise photothermal insecticide

Haijun Wang
Shandong First Medical University and Shandong Academy of Medical Sciences
Qian Zhang
Shandong First Medical University and Shandong Academy of Medical Sciences
Xinyu Zhang
Shandong First Medical University and Shandong Academy of Medical Sciences
Kexin Zhang
Shandong First Medical University and Shandong Academy of Medical Sciences
Xichen Zhao
Shandong First Medical University and Shandong Academy of Medical Sciences
Ruiling Zhang
Shandong First Medical University and Shandong Academy of Medical Sciences
Zhong Zhang (zhangz@sdfmu.edu.cn)
Shandong First Medical University and Shandong Academy of Medical Sciences

Article

Keywords: Polydopamine-coated Fe3O4 nanoplatform, Pesticide-free, Precise photothermal insecticide, Intestinal bacteria, Environmental friendliness

Posted Date: February 15th, 2022

DOI: https://doi.org/10.21203/rs.3.rs-1356519/v1

Abstract

Chemical pesticides are widely used in prevention and control of pests. However, low insecticidal efficacy, high environmental risks and pesticidal resistance severely constrain further applications. In this study, a near-infrared (NIR) laser-activated pesticide-free Fe_3O_4@PDA nanoplatform with a low production cost was constructed for precise photothermal killing of housefly larvae. The polydopamine (PDA) surface-functionalized Fe_3O_4 nanoparticles (Fe_3O_4@PDA NPs) were synthesized by simply mixing dopamine with Fe_3O_4 NPs under aerobic alkaline conditions. These Fe_3O_4@PDA NPs exhibited superb photothermal performance with near-infrared (NIR) laser irradiation. Larval uptake results revealed greater *in vivo* uptake of Fe_3O_4@PDA NPs than bare Fe_3O_4 NPs when housefly larvae were fed a NP-treated diet. These NPs exhibited favorable biocompatibility and showed no obvious influence on larval development and intestinal microbial population. However, when irradiated with a NIR laser, the NPs efficiently induced death of housefly larvae with high temperature (T_{max} > 50 ℃) damage to the intestinal wall and subsequent leakage of intestinal bacteria into the hemocoel. Furthermore, uneaten NPs can be collected by magnetic absorption and show excellent thermal stability, which allowed recycling of these environmentally friendly nanoparticles. The Fe_3O_4-based nanoparticles described in the present study integrate the independence of pesticides, pronounced photothermal control of pests, and environmental friendliness, making this nanoplatform promising for controlling vector pests and diseases.

Introduction

Musca domestica L. (Diptera: Muscidae), a synanthropic fly, can be found in poultry, livestock and human facilities. As a major worldwide pest, they interfere with human life and spread human diseases.

House flies are carriers of more than 65 human and animal intestinal diseases and are responsible for bacterial protozoan and helminthic infections as well as viral and rickettsial infections[1, 2]. These flies also transmit eye diseases such as trachoma, infect wounds and skin with diseases such as cutaneous diphtheria, mycoses, yaws and leprosy[3, 4]. Larvae can invade the human umbilical cord, oral cavity, nasal cavity, intestinal tract, ear canal, eye, pelvic organ and other parts, causing myiasis[5, 6, 7, 8].

The annual cost for insecticides used to control house flies in poultry farms in the United States has been estimated to be over 1.6 million (US dollars)[9]. Adult house flies are often controlled with insecticides when adult fly populations exceed acceptable abundance or activity levels[10]. However, overuse of insecticides for house fly control has resulted in development of house fly resistance to nearly all major insecticide classes[11].

Traditional control methods are currently limited to the use of physical patting, electrocuting light traps, odor baited traps and chemical insecticides (such as carbamates, organophosphates and pyrethroids) to kill house fly adults and larvae[12]. However, the low efficiency and rapid accumulation of dust on sticky materials for these physical control methods severely limit their application. Chemical control is the most

efficient and common strategy used to suppress house fly populations. For example, insecticide-mixed sugars attract house flies and then kill them. However, abuse of chemical pesticides can cause consequent environmental disruption, ecological imbalance, mortality of nontarget organisms and development of pesticide resistance[13, 14]. Furthermore, less than 0.1% of pesticides ultimately act on harmful biological targets due to evaporation, runoff and degradation[15]. Therefore, researchers have sought alternative control strategies.

In recent years, nanopesticide carriers based on organic polymers or inorganic nanoparticles have been widely developed. These nanopesticide carriers reduce the toxic effects of pesticides on the surrounding environment and improve pesticide utilization efficiency by suppressing evaporation and degradation and prolonging the effective duration. For example, Yan *et al*. developed a star polymer (SPc) for delivering a pesticide (osthole) to control both pests and diseases of strawberry. This nanosized osthole/SPc complex was delivered to the cytoplasm of insect cells, and the efficacy for control of strawberry pests and diseases was significantly improved. Moreover, the osthole/SPc complex exhibited no influence on strawberry fruit quality and nontargeted predators, which fulfilled the need for green control of pests[16]. To improve insecticidal efficacy and reduce the environmental risks of pesticides, Luo *et al*. constructed self-assembled degradable nanogels featuring foliar affinity and pinning for pesticide delivery. These pesticide-loaded nanogels increased the foliar protection area and improved both the pesticide exposure area and target contact efficiency. Due to their flexibility and viscosity, the nanogels largely enhanced washing resistance and the retention rate of the pesticide. Moreover, the degradability of nanogels make these nanocarriers environmentally friendly and promising for delivering pesticides[17]. However, chemical control may not be an effective strategy for controlling this double-wing house fly with a wide range of activities, especially outdoors. Furthermore, this nanoscale pesticide still did not break away from classical biological or chemical control techniques and showed potential for pesticide resistance. Therefore, it is necessary to explore new disruptive and precise control strategies.

External/internal stimulus-responsive smart nanoagents featuring precise theranostics have been widely used in different fields. For example, in our previous work, we reported that pH-, GSH- and H_2O_2-responsive MnO_2-based nanoparticles exhibited superb potential for tumor-targeted theranostics[18, 19]. Bo *et al*. developed polydopamine (PDA)-based nanoparticles (NPs) for H_2O_2 removal in the treatment of oxidative stress-induced periodontal disease[20]. Specifically, photothermal materials convert visible to near-infrared (NIR) light into heat, leading to thermal ablation of cells and tissues, and this is a minimally invasive and controllable method that has drawn widespread attention[21, 22]. Moreover, houseflies generally lay eggs in polluted feces, organic waste and other environments, and these develop into housefly larvae. Housefly larvae have a limited range of motion and take up their food through broad scraping, allowing them to take up nanoscale photothermal materials.

In this study, we constructed an NIR-activated Fe_3O_4@PDA nanoplatform for precise photothermal control of housefly larvae to eliminate pesticide dependence. As shown in Scheme 1, environmentally friendly Fe_3O_4 NPs were chosen as the photothermal precursor. Then, a thin PDA layer (also showing high

photothermal conversion efficiency)[23] was coated on the Fe_3O_4 NPs. We evaluated the photoconversion efficiency of Fe_3O_4@PDA NPs *in vitro* and *in vivo*. NIR thermal imaging and inductively coupled plasma–optical emission spectrometry (ICP–OES) were used to investigate the uptake of NPs by housefly larvae. Additionally, the biosafety of NPs for larval development of intestinal microbial populations was studied. Finally, NIR laser-activated thermal control of larvae and its mechanism were systematically studied. The results demonstrated that Fe_3O_4@PDA NPs are promising candidates for controlling vector pests and diseases.

Results And Discussion

Synthesis and characterization of Fe_3O_4@PDA NPs

PDA-functionalized Fe_3O_4 NPs were synthesized *via* dopamine oxidation and self-polymerization. Scanning electron microscopy (SEM) images showed that these organic PDA-coated NPs have rough and flexible surfaces, while the surfaces of bare Fe_3O_4 NPs are relatively smooth and rigid (Fig. 1a, b). Transmission electron microscopy (TEM) images revealed that a thin layer was coated onto the surface of Fe_3O_4 NPs and showed a core/shell morphology (Fig. 1c, d). The average size of the nanoparticles was increased from 183.8 ± 27.5 nm to 201.2 ± 17.0 nm (Supplementary Figure 1). These nanoscale NPs had negligible effects upon uptake by housefly larvae when mixed with feeding materials.

The chemical characteristics of the NPs were examined by Energy-dispersive X-ray spectroscopy (EDS). As shown in Supplementary Figure S2, the signals for Fe were derived from the Fe_3O_4 core, and those for C and N were ascribed to the PDA shell, while elemental Cu in the EDS spectrum probably arose from the copper grid. This result confirmed the presence of PDA. Element mapping indicated the presence of PDA and a uniform distribution in the as-prepared NPs (Fig. 1e–i). FTIR spectroscopy of Fe_3O_4@PDA NPs revealed the appearance of new peaks between 1,000 cm^{-1} and 1,600 cm^{-1} (Supplementary Figure 3): the peak at 1280 cm^{-1} was assigned to aromatic ring absorption; the peaks at 1,500 and 1,600 cm^{-1} were ascribed to N-H shearing vibrations; and a peak at 3,450 cm^{-1} was assigned to intermolecular O-H stretching vibrations or aromatic secondary amine N-H stretching vibrations; these data indicated the presence of PDA[24]. Overall, these results confirmed successful coating of PDA onto the Fe_3O_4 NPs. Finally, the weight percent of Fe_3O_4 in Fe_3O_4@PDA NPs was quantified by ICP–OES and found to be 73.7 ± 2.1%.

Both Fe_3O_4 NPs and Fe_3O_4@PDA NPs absorb broadly at UV and NIR wavelengths (Supplementary Figure 4), so efficient light-to-heat conversion should occur. As expected, both Fe_3O_4 NPs and Fe_3O_4@PDA NPs exhibited strong photothermal performance and displayed temperature increases that depended on the laser power density (Fig. 2a, b). Specifically, the temperature of the Fe_3O_4@PDA NPs (0.5 mg/mL) increased to 73.3 °C (Δt = 45.5 °C) after irradiation (2.0 W/cm^2) for 300 s, which was higher than that

of Fe_3O_4 NPs (T = 68.8 ℃; Δt = 41.9 ℃), while the temperature of DI water was increased by only 8.7 ℃ under the same conditions (Supplementary Figure 5). At low concentrations (≤ 0.5 mg/mL), these two NPs showed concentration-dependent temperature increases with a laser power density of 1 W/cm^2 (Fig. 2 c, d). However, when the concentrations reached 1 mg/mL, the temperatures of the Fe_3O_4 NPs and Fe_3O_4@PDA NPs reached 50 ℃ (Δt = 23.4 ℃) and 52.8 ℃ (Δt = 26.2 ℃), respectively, which were lower than 53.5 ℃ (Δt = 26.3 ℃; Fe_3O_4 NPs) and 57.8 ℃ (Δt = 30.7 ℃; Fe_3O_4@PDA NPs) seen at a concentration of 0.5 mg/mL. This may be ascribed to the tendency for high concentrations of NPs to aggregate at high temperatures, since the thermocouple probe mainly measured the temperature of the supernatant solution. This can also be seen from the results of photothermal heating photographs. As shown in Fig. 2e, the Fe_3O_4@PDA NP dispersion (0.5 mg/mL) showed excellent photothermal stability with no obvious aggregation over five minutes of illumination, while the Fe_3O_4 NP dispersion (0.5 mg/mL) aggregated substantially from the first minute. This excellent photothermal performance indicated high potential for killing housefly larvae.

Biosafety evaluation

These pesticide-free NPs were designed to fulfill the need for green control of pests, so the effects of NPs on body length, body weight, pupal weight, pupation rate and emergence rate of housefly larvae were first systematically evaluated. Varied volume (1, 3, 5, 10 mL) of **F**e$_3$O$_4$ NP suspension (10 mg/mL, in DI water) was mixed with wheat bran and milk powder (Wheat bran (g): DI water (mL): milk powder (g) = 1:1:0.4), this giving feeding materials, and termed **F**1, **F**3, **F**5, **F**10, respectively. **F**e$_3$O$_4$@**P**DA NPs-included feeding materials was mixed used the same mixture ratio, and termed **FP**1, **FP**3 and **FP**5, **FP**10. Ten normal-breeding, good-growing and uniform-sized 1-day-old housefly larvae were fed with F1, F3, F5, F10, FP1, FP3 and FP5, FP10 in gauze covered porous centrifuge tube (10 mL), respectively. During the evaluation period, all housefly larvae were alive. Specifically, compared with the control group, FP1, FP3, FP5 and PF10 showed no effect on the body weights and body lengths of housefly larvae (Fig. 3a, b). Moreover, the pupal weight, pupation rate and emergence rate of larvae fed different doses of Fe_3O_4@PDA NPs were similar to those in the control group (Supplementary Table 1). These results showed that Fe_3O_4@PDA NPs had no significant effects on the development of housefly larvae.

The effect of FP5 on the intestinal microbial population of housefly larvae before and after NIR laser irradiation (808 nm, 1 W/cm^2) was further studied. A total of 14 genera were identified in all housefly larva samples, of which *Providencia* and *Klebsiella* were the dominant genera. The relative abundances of the dominant genus in the intestines of housefly larvae fed FP5 without/with NIR laser irradiation were basically the same as that in the control group (Fig. 3c). Compared with the control group, the relative abundances of *Morganella*, *Weissella* and *Serratia* increased less in the Fe_3O_4@PDA NP (Laser-FP5, Laser+FP5) group, while the relative abundances of *Lactococcus*, *Enterobacter*, *Bordetella* and *Myroides* decreased less (Fig. 3d). According to the heatmap, the compositions of the intestinal flora in different samples of housefly larvae were dynamic. Compared with the nonirradiated group (Laser-CT, Laser-FP5), the relative abundance of *Providencia* increased with Laser + FP51d, Laser + FP52d, and the relative

abundance of *Proteus* and *Myroides* increased with Laser + FP52d, Laser + FP53d. The relative abundances of *Klebsiella*, *Leuconostoc* and *Lactococcus* decreased with Laser+FP51d (Fig. 3d). Principal component analysis (PCA) showed that samples of housefly larvae fed at the same time clustered together, and there were differences in intestinal flora among samples fed at different times (Fig. 3e). UPGMA evolutionary tree analysis further proved that there were differences in intestinal flora between the nonirradiated group (Laser-CT, Laser-FP5) and the irradiated group (Laser + CT, Laser + FP5) (Figure 3f) of housefly larvae. The above results showed that Fe_3O_4@PDA NPs had no effect on the intestinal flora of housefly larvae, but NIR laser irradiation had different effects on the intestinal flora of housefly larvae.

In vivo uptake evaluation

Larval uptake experiments were performed to explore the influence of the PDA functional coating on inorganic Fe_3O_4 NPs on uptake by housefly larvae. ICP–OES quantification results (Fig. 4a) showed a concentration-dependent uptake increase for both Fe_3O_4 NPs and Fe_3O_4@PDA NPs. It was very encouraging to see that the uptake of NPs was significantly increased after coating PDA on the Fe_3O_4 NPs. This was also confirmed by comparing the body colors of larvae. As shown in Fig. 4b–f, the larvae fed FP5 exhibited the darkest color (representing the highest level of uptake), which corresponded to the ICP-OES results. The mechanism may be ascribed to the relatively flexible and adhesive surfaces provided by PDA[25, 26], which helped larvae scrape these NPs.

In vivo photothermal imaging and insecticidal activity evaluation

Inspired by the excellent photothermal performance and enhanced uptake of Fe_3O_4@PDA NPs *in vitro*, *in vivo* photothermal imaging was assessed. Housefly larvae were fed F5 and FP5 and then exposed to an 808 nm NIR laser (1.0 W/cm^2) at 2 d post-feeding. NIR images were captured with an infrared thermal imaging system. As shown in Fig. 5a and Supplementary Figure 6, F5 quickly elevated the temperature of the larvae to 43.6 ℃ within 30 s, and the temperature reached 45.1 ℃ after NIR irradiation for 3 min; the temperature of larvae fed NP-free materials increased by no more than 1 ℃. More encouragingly, FP5 achieved the most potent light-to-heat conversion *in vivo*. The temperature of FP5-fed larvae increased to 51.1 ℃ in the first 30 s, and by the end of irradiation, the temperature reached 52.7 ℃. These results indicated that the Fe_3O_4@PDA NPs have potent *in vivo* photothermal activity and could be used to ablate larval tissue.

The *in vivo* thermal ablation activities occurring in NP-fed larvae were then assessed. After feeding different doses of Fe_3O_4 and Fe_3O_4@PDA NPs, the larvae were irradiated with an NIR laser (1 W/cm^2) at predetermined times (1, 2, 3, or 4 days post-feeding), and the time to death (t_d) was recorded. Generally, in the first two days, the NPs showed feeding time- and dose-dependent insecticidal efficacy, and FP5 achieved the most potent insecticidal efficacy (Fig. 5b, c), while NIR laser irradiation alone did not have any significant insecticidal effects. Specifically, with NIR laser irradiation at 1 day post-feeding, the t_d of F1-, FP1-, F3-, FP3-, F5-, and FP5-fed larvae were 240 s, 240 s, 240 s, 238.6 s, 171.6 s, 149.8 s, and 105 s,

respectively, which were longer than the t_d for 2-day-old larvae after feeding with the corresponding NPs. This may be ascribed to the enhanced uptake ability of 2-day-old larvae, which produced more heat to kill larvae. However, NPs-fed 3-day-old larvae showed weaker insecticidal efficacy (Fig. 5d, e), which was ascribed to decreasing uptake and increasing excretion by 3-day-old larvae. As a result, we chose 2 days of F5- and FP5-fed larvae to further study the effect of power densities on insecticidal efficacy.

With increasing larval feeding time, the death time of larvae was shortened by NIR laser irradiation, and the shortest time of larval death was 2 d (Fig. 5f, g). Similarly, because the uptake amounts for NPs decreased and the excretion amount increased with further development of larvae, the t_d was prolonged for 3-day-old and 4-day-old larvae (Fig. 5h, i).

Insecticidal mechanisms study

To better understand the insecticidal mechanism, a histological analysis were carried out. H&E-stained images of F5- and FP5-fed larvae without NIR laser irradiation showed no obvious intestinal tissue damage compared with those of the control group without/with NIR laser irradiation (Fig. 6a). In sharp contrast, with NIR laser irradiation, F5 caused serious intestinal tissue damage as a result of excellent light-to-heat conversion by Fe_3O_4-based NPs. Moreover, after PDA coating, FP5 further damaged the intestinal tissue, persuasively demonstrating enhanced uptake of NPs by larvae.

Intestinal bacteria have a profound influence on the growth of larvae[27, 28] and may leak into hemocoel when intestinal tissue is damaged. The spilled body fluids of F5- and FP5-fed larvae with/without NIR laser irradiation were cultured by the plate method. As expected, no colonies grew on nutrient agar plates for any of the groups without NIR laser irradiation and the group treated with NIR laser irradiation alone, meaning that no intestinal bacteria leaked into the hemocoel (Fig. 6b). However, the nutrient agar plates from the irradiated housefly larvae groups (Laser+F5, Laser+FP5) were covered with different colonies, indicating leakage of bacteria from the intestinal tract into the hemocoel. Collective thermal ablation of the intestinal tract followed by leakage of intestinal bacteria contributed to the deaths of larvae.

Recovery of NPs

Good biocompatibility and recoverability play key roles in green prevention and control of insect pests. With the revelation that Fe_3O_4-based NPs possess various advantages, including good biosafety and magnetic properties, we recovered Fe_3O_4@PDA NPs by magnetic absorption. The recovery rates were 50.2 ± 7.5% and 27.9 ± 8.0% for F5 and FP5, respectively, further confirming the enhanced uptake of PDA-coated Fe_3O_4 NPs. The photothermal properties and stabilities of the recycled Fe_3O_4@PDA NPs were investigated. As expected, the temperature of the Fe_3O_4@PDA NPs (0.5 mg/mL) also increased to ~59 °C after irradiation (1.0 W/cm^2) for 300 s (Supplementary Figure 7). Furthermore, the recycled Fe_3O_4@PDA NPs possessed desirable photothermal stability for at least three cycles of laser irradiation/cooling

(Supplementary Figure 8), suggesting that Fe_3O_4@PDA NPs may be suitable for use as photothermal insecticides.

To date, the use of pesticides is the most effective and valuable way to decrease the population of house flies. However, the consequent environmental disruption, ecological imbalance, and mortality of nontarget organisms caused by excessive abuse of chemical pesticides severely limits their use. Furthermore, this chemical control effect on adult flies is relatively nonideal, and houseflies easily develop pesticide resistance. Nanopesticide carriers could improve pesticide utilization efficiency and improve the bioavailability of pesticides in the surrounding environment, thus providing an effective, safe, and environmentally friendly way to use pesticides[29, 30]. Based on this nanoscale platform and breaking out the dependence on pesticides, we constructed an NIR laser-activated pesticide-free Fe_3O_4@PDA nanoplatform with a low production cost for precise photothermal control of housefly larvae and provided a new concept for transforming pest control.

Conclusion

In this study, we constructed an NIR-activated pesticide-free Fe_3O_4@PDA nanoplatform for precise photothermal control of housefly larvae. The Fe_3O_4@PDA NPs showed a core/shell morphology with an average size of 201.2 ± 17.0 nm. These Fe_3O_4@PDA NPs exhibited superb photothermal performance with NIR laser irradiation. Larval uptake results revealed greater *in vivo* uptake of Fe_3O_4@PDA NPs than bare Fe_3O_4 NPs when housefly larvae were fed the NP-treated diet. These NPs have favorable biocompatibility and showed no obvious influence on larval development and the intestinal microbial population. However, when irradiated with a NIR laser, the NPs efficiently eliminate housefly larvae due to intestinal wall damage caused by hyperthermia (T_{max} > 50 ℃) and subsequent leakage of intestinal bacteria into the hemocoel. Furthermore, uneaten NPs can be collected by magnetic absorption and show excellent thermal stability, thus allowing recycling of these environmentally friendly nanoparticles. The Fe_3O_4-based nanoparticles described in the present study integrate the independence of pesticides, pronounced photothermal control of pests, and environmental friendliness, making this nanoplatform promising for controlling vector pests and diseases.

Declarations

Data availability. Experimental procedure and characterization data are available in Supplementary Information.

Acknowledgements

We acknowledge the funding provided by the National Natural Science Foundation of China (Nos. 81572028) and the Youth Outstanding Reserve Talents Program of Shandong First Medical University and Shandong Academy of Medical Sciences.

Author contributions

H.W. and Q.Z. contributed equally to this work. H.W. and Z.Z. conceived the project. H.W. prepared and characterized the Fe_3O_4@PDA NPs. H.W., Q.Z., Z.Z. analyzed the data and drafted the manuscript. X.Z., K.Z., X.Z., and R.Z. assisted with the *in vitro* and *in vivo* experiments. All authors read and approved the final manuscript.

Competing interests

The authors declare no competing interests.

References

1. Songe MM, Hang'ombe BM, Knight-Jones TJ, Grace DJIjoer, health p. Antimicrobial resistant enteropathogenic Escherichia coli and Salmonella spp. in houseflies infesting fish in food markets in Zambia. Int. J. Env. Res. Pub. He. **14**, 21 (2017).
2. Ramesh A, *et al.* The impact of climate on the abundance of Musca sorbens, the vector of trachoma. Parasite. Vector. **9**, 1–13 (2016).
3. Robinson A, *et al.* Towards an odour-baited trap to control Musca sorbens, the putative vector of trachoma. Sci. Rep. **11**, 1–11 (2021).
4. Keiding J, Organization WH. The house-fly: biology and control. World Health Organization (1986).
5. Mizumoto J, Yamamoto MJJoG, Medicine F. Intestinal myiasis in a very elderly patient with inappropriate home care. J. Gen. Fam. Med. **20**, 154–156 (2019).
6. Rossi-Schneider T, Cherubini K, Yurgel LS, Salum F, Figueiredo MAJJoos. Oral myiasis: a case report. J. Oral Sci. **49**, 85–88 (2007).
7. Tay SY, Ramasamy BR, Watson DA, Montoya MJCR. Treatment of nasal myiasis with ivermectin irrigation. *Case Reports* 2018, bcr-2017-224142 (2018).
8. Ahmed SS, Ahmed W, Bey AJIJoCPD. Myiasis of maxilla: report of a case. International Journal of Clinical Pediatric Dentistry **4**, 248 (2011).
9. Crespo DC, Lecuona RE, Hogsette JAJBC. Biological Control: An Important Component in Integrated Management of Musca domestica(Diptera: Muscidae) in Caged-Layer Poultry Houses in Buenos Aires, Argentina. Biol. Control **13**, 16–24 (1998).
10. Gerry ACJJoEE. Review of Methods to Monitor House Fly (Musca domestica) Abundance and Activity. J. Econ. Entomol. **113**, 2571–2580, (2020).
11. Freeman JC, Ross DH, Scott JGJPB, Physiology. Insecticide resistance monitoring of house fly populations from the United States. Pestic. Biochem. Phys. **158**, 61–68. (2019).
12. Sarwar K, Iqbal W, Azam I, Malik MFJJOE, STUDIES Z. Role of housefly (Musca domestica, Diptera; Muscidae) as a disease vector; a review. Journal of Entomology and Zoology studies **2**, 159–163 (2014).

13. Malik A, Singh N, Satya SJJoes, B hp. House fly (Musca domestica): a review of control strategies for a challenging pest. *J. Environ. Sci. Heal. B.* **42**, 453–469 (2007).
14. Zhang Z, *et al.* Toxicities of monoterpenes against housefly, Musca domestica L.(Diptera: Muscidae). Environ. Sci. Pollut. R. **24**, 24708–24713 (2017).
15. Liang Y, Fan C, Dong H, Zhang W, Cao YJASC, Engineering. Preparation of MSNs-Chitosan@Prochloraz Nanoparticles for Reducing Toxicity and Improving Release Properties of Prochloraz. ACS Sustain. Chem. Eng. **6**, 10211–10220. (2018).
16. Yan S, *et al.* Simple Osthole/Nanocarrier Pesticide Efficiently Controls Both Pests and Diseases Fulfilling the Need of Green Production of Strawberry. ACS Appl. Mater. Interfaces **13**, 36350–36360 (2021).
17. Luo J, *et al.* Self-Assembled Degradable Nanogels Provide Foliar Affinity and Pinning for Pesticide Delivery by Flexibility and Adhesiveness Adjustment. ACS Nano, **15**, 14598–14609 (2021).
18. Wang H, *et al.* Platelet membrane biomimetic bufalin-loaded hollow MnO_2 nanoparticles for MRI-guided chemo-chemodynamic combined therapy of cancer. Chem. Eng. J. **382**, 122848 (2020).
19. Wang H, *et al.* Dimeric Her2-specific affibody mediated cisplatin-loaded nanoparticles for tumor enhanced chemo-radiotherapy. J. Nanobiotechnol. **19**, 138 (2021).
20. Bao X, Zhao J, Sun J, Hu M, Yang X. Polydopamine Nanoparticles as Efficient Scavengers for Reactive Oxygen Species in Periodontal Disease. ACS Nano **12**, 8882–8892 (2018).
21. Wang H, Williams GR, Xie X, Wu M, Wu J, Zhu L-M. Stealth Polydopamine-Based Nanoparticles with Red Blood Cell Membrane for the Chemo-Photothermal Therapy of Cancer. ACS Appl. Bio Mater. **3**, 2350–2359 (2020).
22. Yang Q, *et al.* Porous Au@Pt Nanoparticles: Therapeutic Platform for Tumor Chemo-Photothermal Co-Therapy and Alleviating Doxorubicin-Induced Oxidative Damage. ACS Appl. Mater. Interfaces **10**, 150–164 (2018).
23. Han X, *et al.* An Extendable Star-Like Nanoplatform for Functional and Anatomical Imaging-Guided Photothermal Oncotherapy. ACS Nano **13**, 4379–4391 (2019).
24. Chen W, Qin M, Chen X, Wang Q, Zhang Z, Sun X. Combining photothermal therapy and immunotherapy against melanoma by polydopamine-coated Al_2O_3 nanoparticles. Theranostics **8**, 2229–2241 (2018).
25. Zhang L, Wu J, Wang Y, Long Y, Zhao N, Xu J. Combination of bioinspiration: a general route to superhydrophobic particles. J. Am. Chem. Soc. **134**, 9879–9881 (2012).
26. Lee H, Dellatore SM, Miller WM, Messersmith PBJs. Mussel-inspired surface chemistry for multifunctional coatings. Science **318**, 426–430 (2007).
27. Behar A, Yuval B, Jurkevitch EJJoIP. Gut bacterial communities in the Mediterranean fruit fly (Ceratitis capitata) and their impact on host longevity. J. Insect. Physiol. **54**, 1377–1383 (2008).
28. Augustinos AA, Kyritsis GA, Papadopoulos NT, Abd-Alla AM, Cáceres C, Bourtzis KJPo. Exploitation of the medfly gut microbiota for the enhancement of sterile insect technique: use of Enterobacter sp. in

larval diet-based probiotic applications. Plos One **10**, e0136459 (2015).

29. Feng J, *et al.* Development and Characterization of Pyriproxyfen-Loaded Nanoemulsion for Housefly Control: Improving Activity, Reducing Toxicity, and Protecting Ecological Environment. ACS Sustain. Chem. Eng. **9**, 4988–4999 (2021).
30. Mahyoub JA. Bioactivity of two marine algae extracts and their synthesized silver nanoparticles as safe controls against Musca domestica housefly. Entomol. Res. **51**, 323–330 (2021).

Schemes

Scheme 1 is in the supplementary files section.

Figures

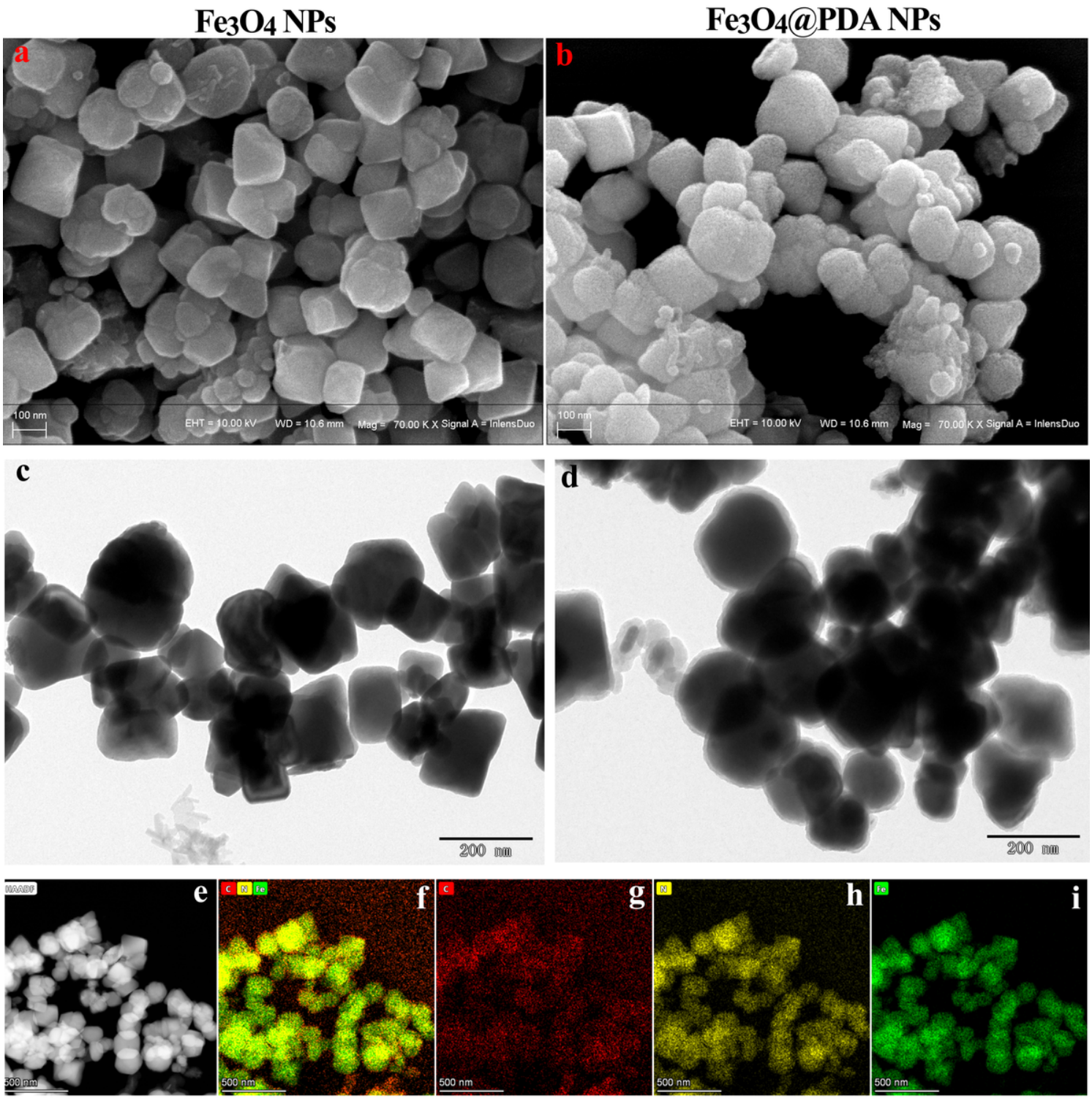

Figure 1

SEM images of (a) Fe_3O_4 NPs and (b) Fe_3O_4@PDA NPs. TEM images of (c) Fe_3O_4 NPs and (d) Fe_3O_4@PDA NPs. (e) HAADF-STEM images of Fe_3O_4@PDA NPs. Elemental mapping of Fe_3O_4@PDA NPs: (f) merged image, (g) C, (h) N and (i) Fe.

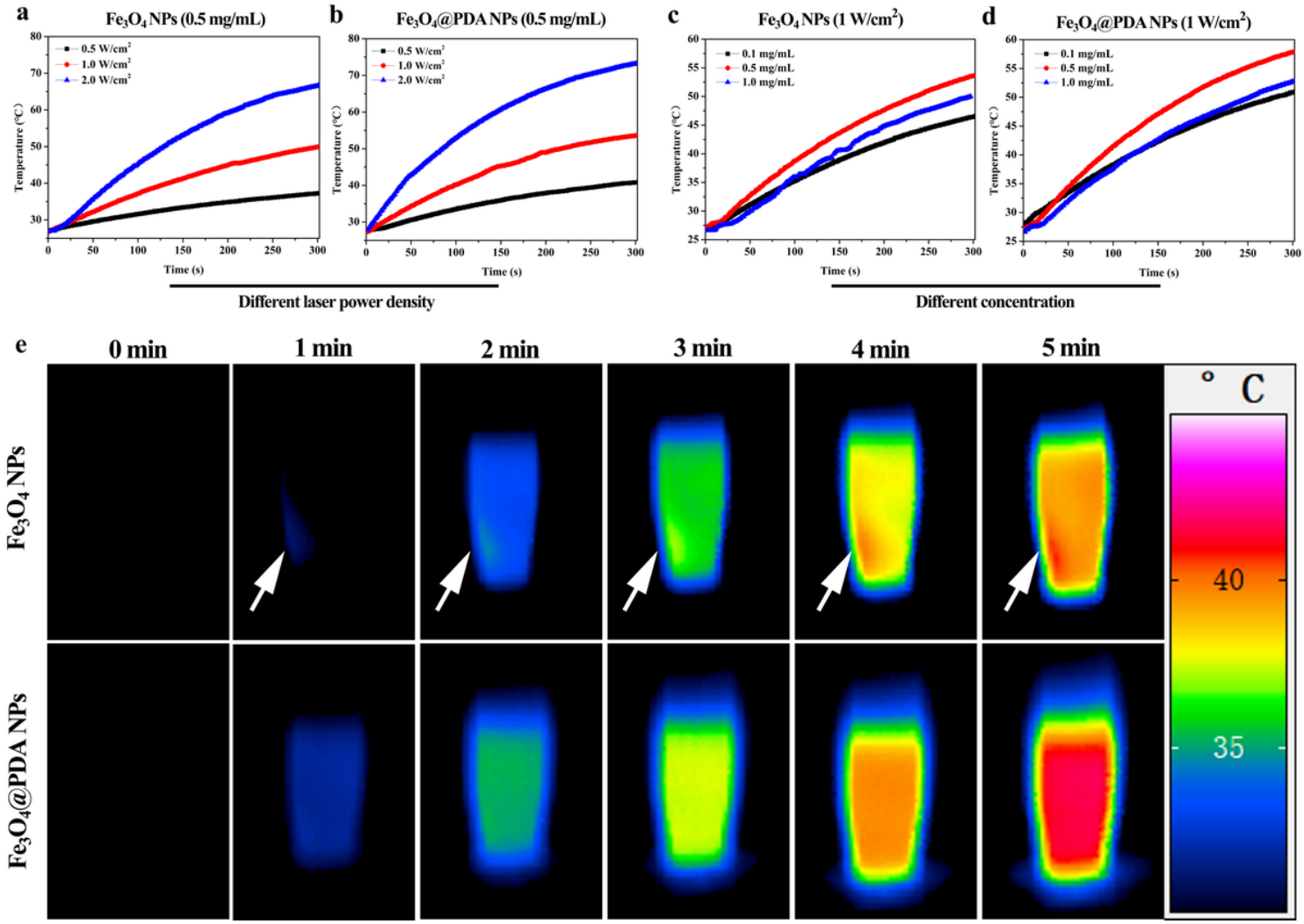

Figure 2

Temperature vs. time plots for (a) Fe_3O_4 NP and (b) Fe_3O_4@PDA NP suspensions with a laser power density of 0.5 mg/mL. Temperature vs. time plots for (c) Fe_3O_4 NP and (d) Fe_3O_4@PDA NP suspensions at different concentrations with a laser power density of 1 W/cm^2 for 5 min. (e) Photothermal images for Fe_3O_4 NP and Fe_3O_4@PDA NP suspensions (0.5 mg/mL) under continuous NIR laser irradiation (1 W/cm^2) for 5 min. The white arrows indicate aggregation.

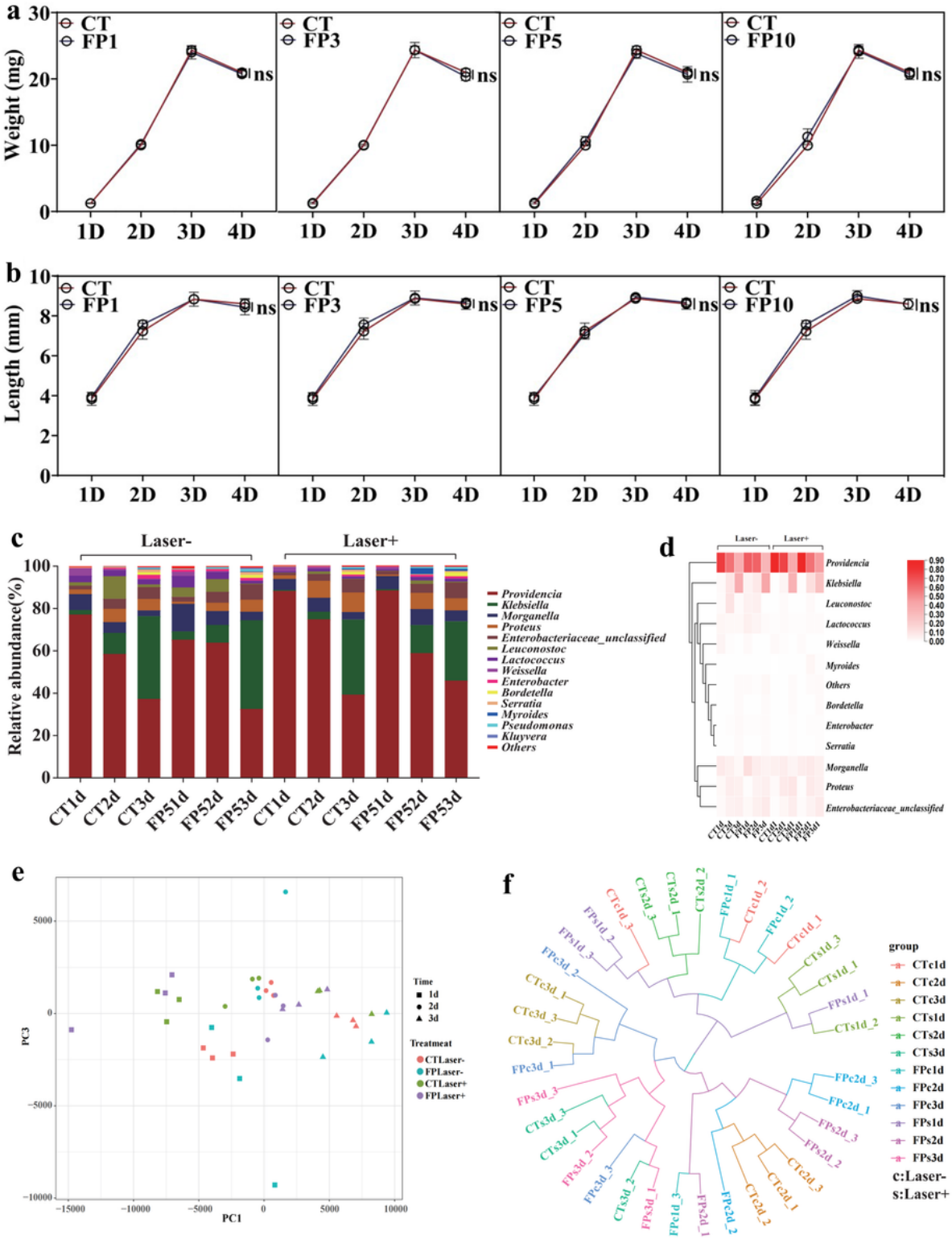

Figure 3

Effects of different Fe_3O_4@PDA NP doses on the growth and development of housefly larvae. (a) Body lengths and weights of housefly larvae; (b) Housefly pupae weights. CT: sterile water. Repeated measures ANOVA followed by Sidak correction was used for multiple comparisons. *$p < 0.05$, **$p < 0.01$, ***$p < 0.001$. Effects of Fe_3O_4@PDA NPs on the gut microbiota of housefly larvae. (c) Relative abundance of bacterial components in the intestines of housefly larvae before and after NIR laser irradiation. Each

treatment included three biological replicates. (d) Heatmaps of relative abundances and distributions of bacterial genera in housefly larvae. Heatmap based on the bacterial genera of different groups and color coded by genus following the legend in the panel. (e) Principal component analysis (PCA) of bacterial community structures for different groups. Each symbol represents one sample of intestinal bacteria. (f) UPGMA evolutionary tree analyses of samples. Laser-: before NIR laser irradiation; Laster+: after NIR laser irradiation. 1 d, 2 d and 3 d represent the development times of housefly larvae.

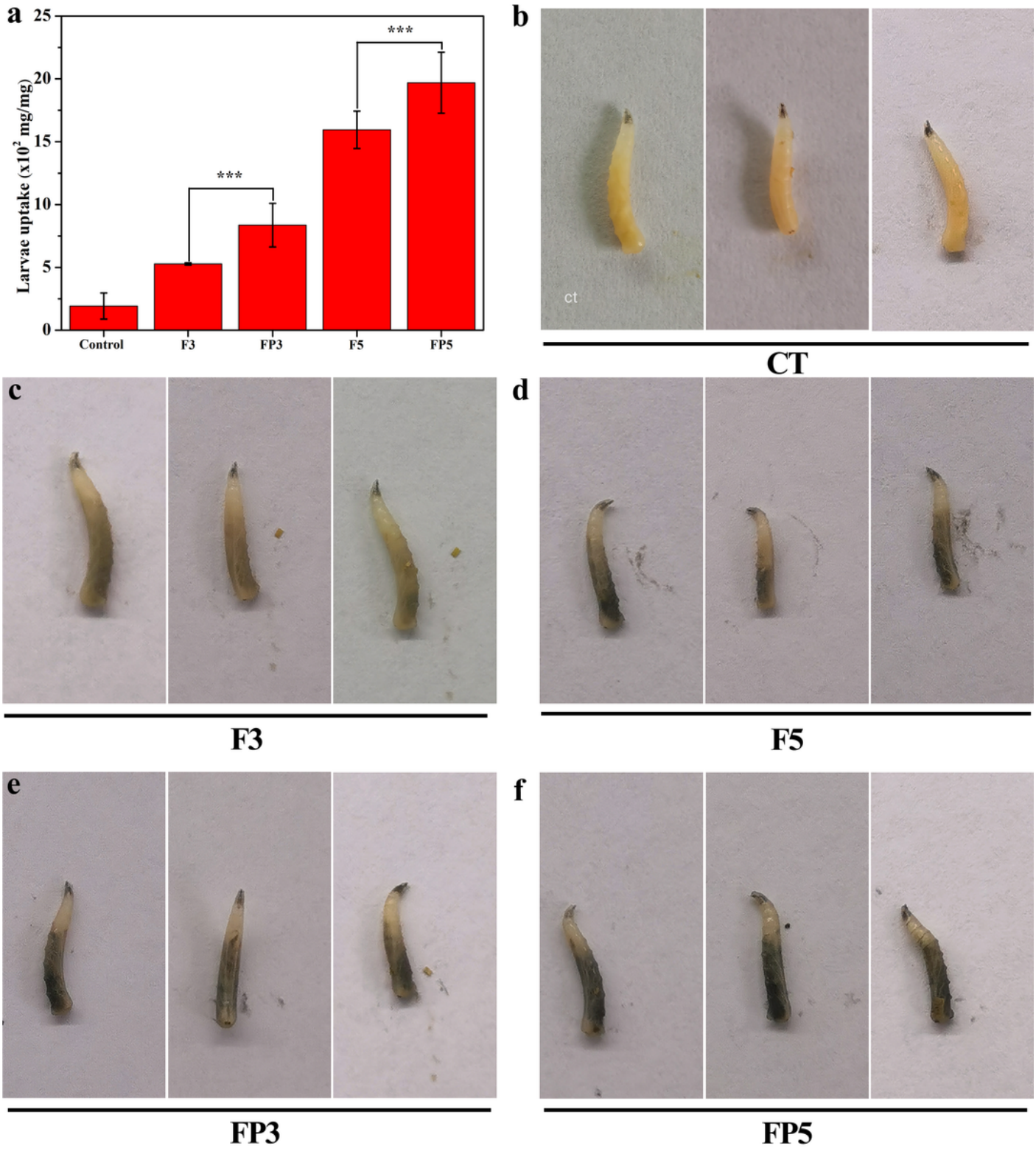

Figure 4

(a) Uptake data for F3 vs. FP3, F5 vs. FP5. Data are reported as the ratio of Fe content in larvae to the body weight. Representative photographic image of (b) control larvae and larvae after feeding with (c) F3, (d) F5, (e) FP3, and (f) FP5 for two days. NP-free feeding materials were used to feed larvae serving as controls.

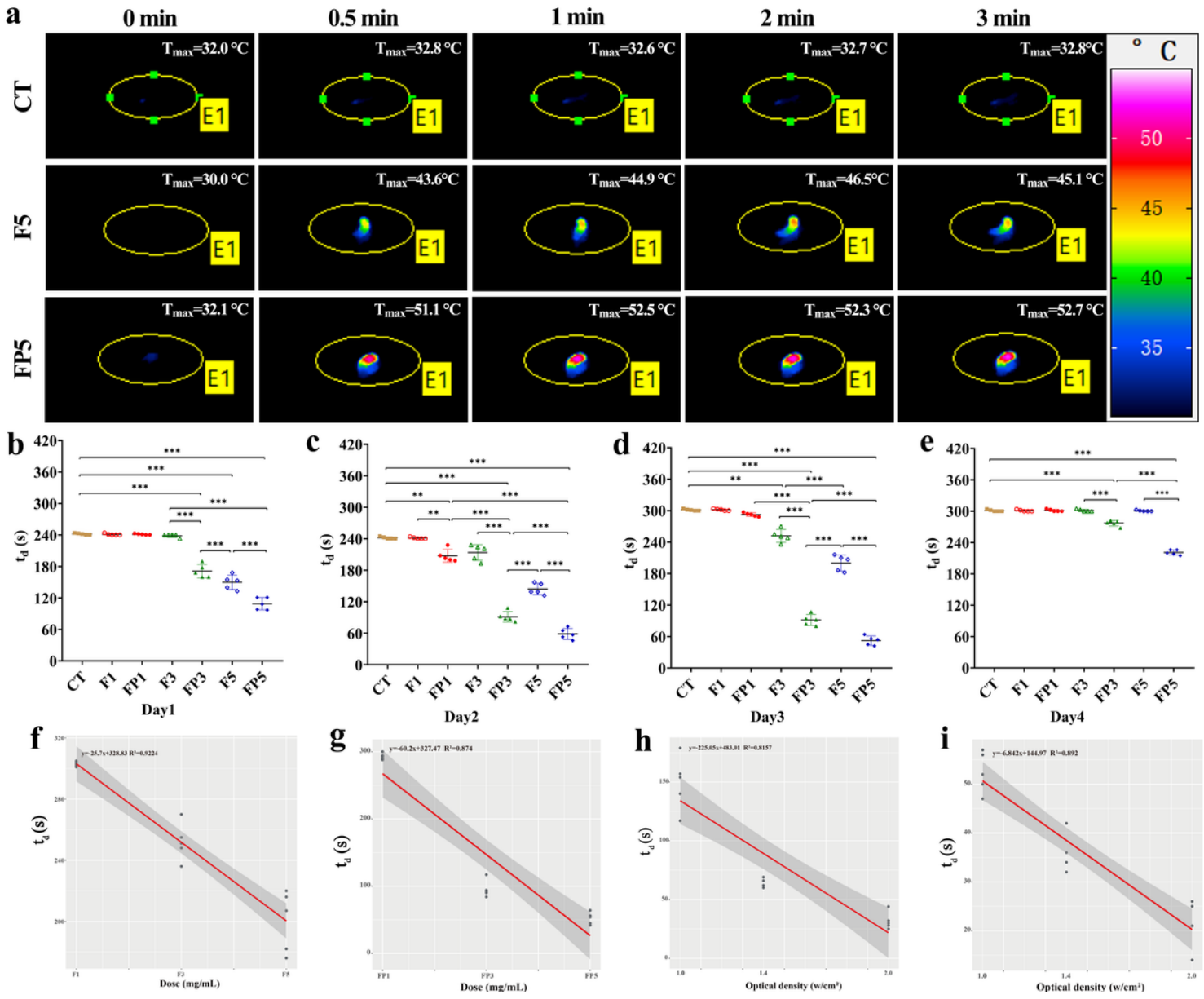

Figure 5

(a) Thermal images of F5 and FP5-fed larvae after exposure to NIR irradiation for 3 min (1 W/cm^2). The time of larval death (t_d) after irradiation by an NIR laser for houseflies fed with different doses of Fe_3O_4 and Fe_3O_4@PDA NPs: (b), (c), (d), (e) represent the development times of the larva. Correlation between the death time of larvae irradiated by the NIR laser and the doses of (f) Fe_3O_4 and (g) Fe_3O_4@PDA NPs; correlation between the death time of larvae fed with (h) Fe_3O_4 and (i) Fe_3O_4@PDA NPs and irradiated by

the NIR laser with different optical densities. CT: sterile water. The data were compared by using one-way ANOVA. Significance analysis was performed with Fisher's LSD test. *$p < 0.05$, **$p < 0.01$, ***$p < 0.001$. Each treatment included five biological replicates.

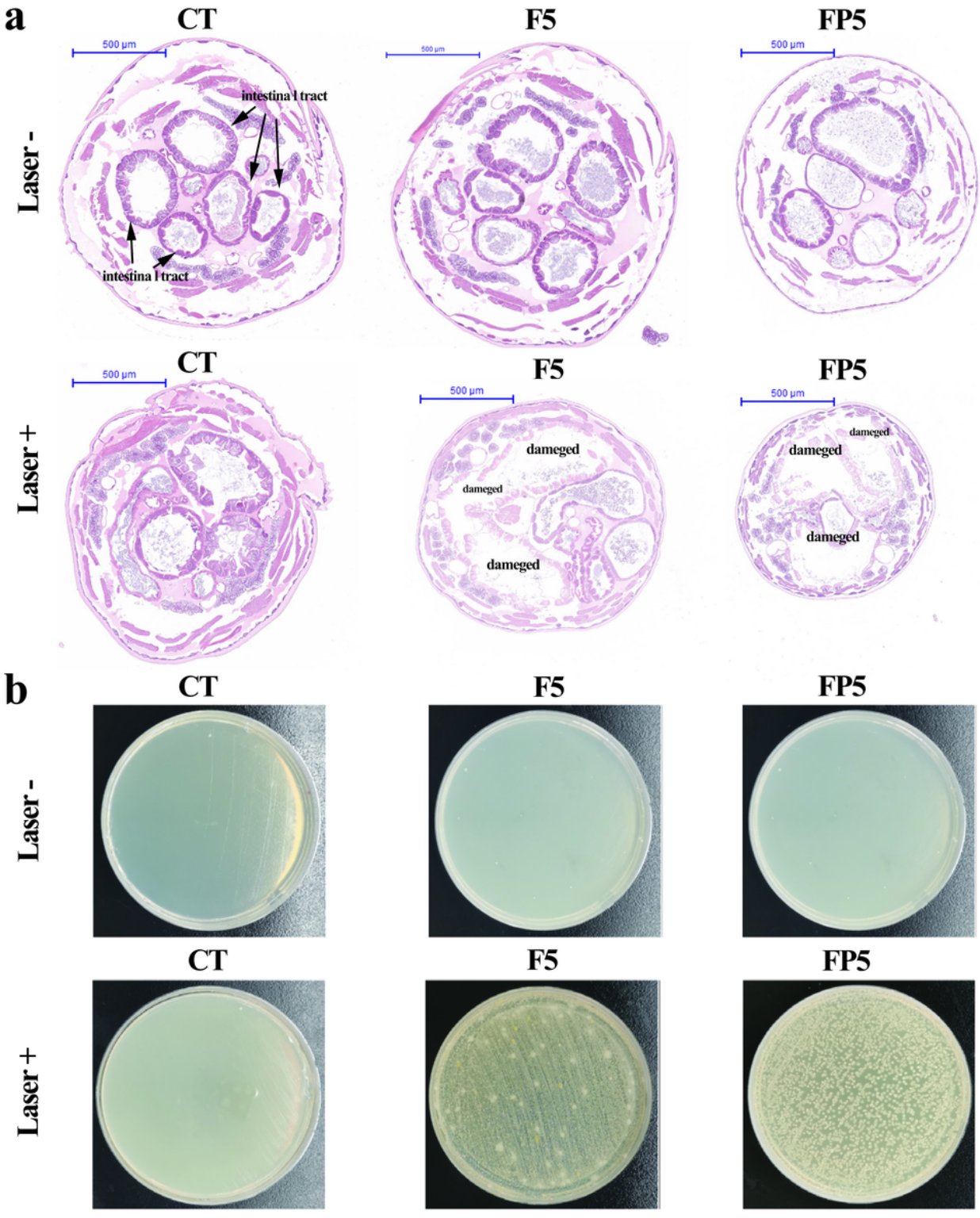

Figure 6

(a) Representative H&E-stained images and (b) intestinal bacterial leakage tests of larvae collected before and after NIR laser irradiation. Each treatment included three biological replicates. CT: sterile water. Laser-: before NIR laser irradiation; Laster+: after NIR laser irradiation.

Supplementary Files

This is a list of supplementary files associated with this preprint. Click to download.

- SupplementaryinformationNC.docx
- floatimage1.png